Progress In Electromagnetics Research C, Vol. 50, 65–74, 2014

Characterization and Design of Millimeter-Wave Full-Band Waveguide-Based Spatial Power Divider/Combiner

Kang Yin[1, *], Kedi Zhang[2], and Jin-Ping Xu[1]

Abstract—The design and implementation of millimeter-wave full-band waveguide-based spatial power divider/combiner are presented in this paper. The divider/combiner is based on a compact waveguide-to-microstrip (Wg-Ms) probe-array transition structure, providing full-band frequency coverage and low insertion loss. Efficient design and analysis method for this type of power divider/combiner is developed using spectral domain method combined with the image theory. Ka-band two-way (1×2) and four-way (2×2) power combining structures are analyzed and optimized. The performances of the both optimized power dividers/combiners are evaluated by experiments in back-to-back configurations. The measured overall insertion loss for the 1×2 power divider/combiner is better than 1.4 dB over the entire Ka-band, which demonstrates the low-loss performance of the divdier/combiner. The optimized 2×2 power divider/combiner shows a same performance as the 1×2 structure without any degradation in operating bandwidth and insertion loss.

1. INTRODUCTION

Millimeter-wave solid-state power amplifiers with broadband and high power are gaining more interest in many applications such as measurement systems, electronic warfare systems, and communication systems. For millimeter-wave systems, the output power from a single broadband solid-state device is often not enough. Therefore, it is necessary to combine power from multiple devices to obtain the desired power level. A variety of power combining techniques has been reported at microwave and millimeter-wave frequencies [1–13]. Conventional binary networks based on planar transmission line such as the Wilkinson power divider and Lange coupler [1–3] suffer from high loss. Waveguide based magic-Tee [4] and branch line are two well known low-loss combining schemes in millimeter wave. However, the whole system will become rather bulky with the increasing number of devices. Spatial or quasi-optical power combining is a promising approach that integrates large number of devices to get high power at millimeter-wave frequencies [5–13]. In these designs, the output power from multi-device is added in air or a single-mode waveguide using a single stage of power combining with parallel manner. A remarkable advantage of this approach is that the loss tends to be fixed and independent of the number of devices. The free-space power-combined amplifiers have been reported in a grid configuration [6], or using conventional planar antennas [7, 8]. In these cases, the active devices are spaced in a single layer transverse to the wave propagation, making it difficult to dissipate the heat. Furthermore, since small resonant antennas are used to divide and combine power in free-space, this approach often exhibits a limited bandwidth and suffers from radiation losses, focusing errors, and the problems of input/output isolation. In order to eliminate these problems, waveguide-based spatial power dividers/combiners, where power combining occurs in closed waveguide or coaxial waveguide, are intensively studied [9–13]. Most of the reported power divider/combiners [9–12], in spite of their

Received 16 March 2014, Accepted 2 May 2014, Scheduled 9 May 2014
* Corresponding author: Kang Yin (yinkang_1@hotmail.com).
[1] State Key Laboratory of Millimeter Waves, Southeast University, Nanjing 210096, China. [2] Department of Electrical and Computer Engineering, University of Illinois at Urbana-Champaign, Urbana, IL 61801, USA.

wideband performance, are mainly used in microwave frequency band. The small cross-sectional size of waveguide and difficulty in dissipating heat limit their applications in millimeter-wave frequency. Recently, a waveguide-based spatial power-combined amplifier using Wg-Ms E-plane dual-probe was developed in millimeter-wave frequency [13]. In this design, low loss E-plane microstrip dual-probe is utilized to achieve waveguide-to-microstrip transition and power dividing/combining simultaneously. They demonstrated a Ka-band four-way power-combined amplifier with combining efficiency more than 77% from 32 to 37 GHz. However, in this structure, the dual-probe and high power PAs are arranged in a common cavity with a face to face configuration. From the reliability point of view, the low spatial isolation would cause some undesirable mutual interference between the PAs, which degrade the circuit performance and even produce oscillating. Furthermore, the relatively large aperture through which the dual-probe is inserted into the waveguide influences on the distribution of electromagnetic field in the waveguide and limits the operating bandwidth.

In this paper, we present the characterization and design of two millimeter-wave full-band waveguide-based spatial power dividers/combiners, which are based on an improved Wg-Ms probe-array transition. Efforts have been devoted to improvement on combining efficiency, extending on frequency coverage and efficient optimization of the passive structures. In the 2×2 divider/combiner, the dual probes are inserted into waveguide through separated small apertures and the active devices are shielded in separated cavities. The structure, therefore, allows improved insertion loss and reliability. In addition, generalized closed-form expression for the input impedance of the probe-array is obtained using spectral domain method, which can be used to analyze and synthesize the power divider/combiner efficiently. The detailed modeling and design of the proposed 1×2 and 2×2 dividers/combiners are discussed in Section 2. Fabrication and experimental results of the dividers/combiners are presented in Section 3. A brief summary and conclusion are given in Section 4.

2. MODELING AND DESIGN

The configuration of the 1×2 power divider/combiner is depicted in Figure 1(a). It can be seen as an extension of the single Wg-Ms probe [14]. Two identical probes are anti-symmetrically inserted into the waveguide through apertures in broad-wall from two opposite directions. The 1×2 power divider/combiner can also be extended to 2×2 divider/combiner by vertical stacking inside the waveguide with a face-to-face configuration, as shown in Figure 1(b). For broadband applications, the apertures are kept as small as possible to prevent propagation of waveguide modes into the microstrip channels. The waveguide is terminated with a back-short located at approximately 1/4 wavelength from the probes. At each of the probe feed-point, a high impedance line is used to achieve broadband matching of the probe impedance to a 50-ohm microstrip line. Both of the divider/combiner exhibit excellent uniform power dividing characteristic. The transmission between the microstrip ports placed on the same side is in phase while the transmission between the ports on the different sides is out of phase. It is because the electric fields of TE_{10} mode induce anti-symmetrical currents on the probes. This characteristic

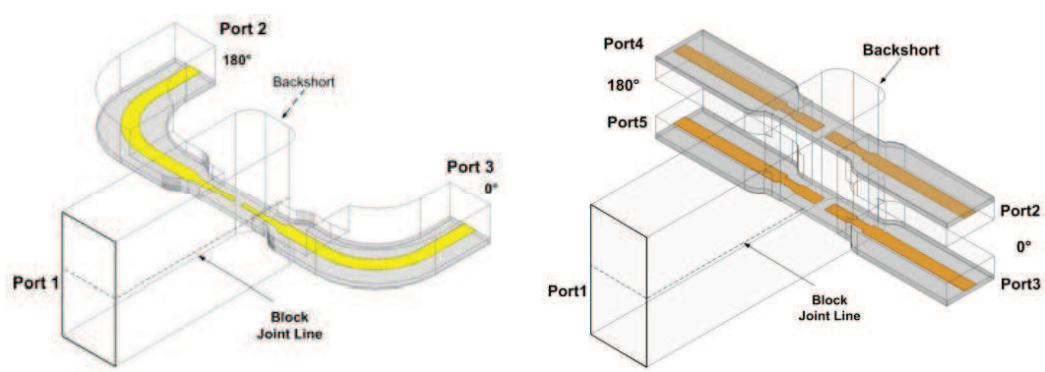

(a) (b)

Figure 1. Structures of the power divider/combiner. (a) 1×2 structure. (b) 2×2 structure.

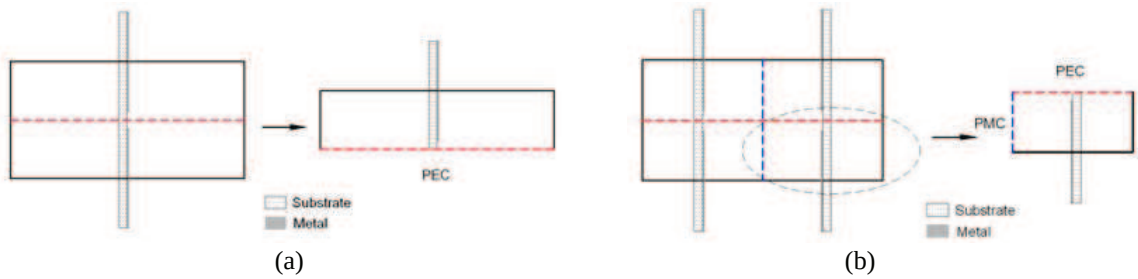

Figure 2. Simplified models of (a) 1×2 structure with PEC, (b) 2×2 structure with PEC-PMC.

is an intrinsic property regardless of frequency and only determined by the symmetrical structure. In the 2×2 divider/combiner, the face-to-face probe pairs are inserted into waveguide through separated small apertures and the PAs are shielded in separated channels to get high spatial isolation. As can be seen later, this is very important for realizing high performance and stable full-band power combining network.

In fact, due to the symmetry in the structure and the dominant TE_{10} mode excitation, the image theory can be used to reduce the design process and simulation time. The 1×2 power divider can be simplified to a single Wg-Ms probe with perfect electric conductor boundary condition (defined as PEC) applied on the H-plane, as shown in Figure 2(a). The 2×2 divider can be simplified with a perfect electric conductor together with a perfect magnetic conductor boundary condition (defined as PEC-PMC), applied on the H-plane an E-plane, respectively, as shown in Figure 2(b). Then the problem of matching the power divider is confined to matching a microstrip probe in a rectangular waveguide with specific boundary conditions.

2.1. Input Impendence of a Microstrip Probe in Waveguide

In this paper, the spectral-domain dyadic Green's function in a rectangular waveguide with specific boundary conditions is derived using spectral domain immitance approach [15], and the basic technique reported by G. Yassin [16] is developed further to produce a general analytical expression for the input impedance of the single microstrip probe with different boundary conditions.

Figure 3(a) shows the generalized model of the single microstrip probe in waveguide. The equivalent-circuit model is shown in Figure 3(b). The length and width of the probe are denoted by x_1 and $2w$, respectively. Distance from the center of the probe to the back-short is z_1. PEC planes

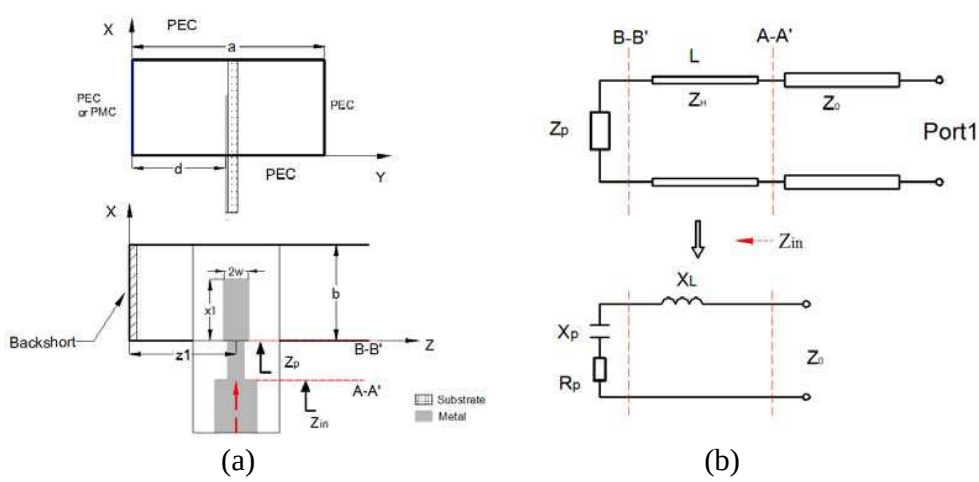

Figure 3. Simple model of a single Wg-Ms probe with different boundary conditions. (a) Geometry. (b) Equivalent circuit.

are located at $x = 0$, $x = b$ and $y = a$. PEC or PMC plane are locate at $y = 0$. The input impedance Z_p is calculated from the given equation [16]:

$$Z_p = \frac{2}{b}\sum_{n=0}^{+\infty}\delta_n \sum_{m=1}^{+\infty}\lim_{\beta\to\beta_{mn}}\left\{(\beta-\beta_{mn})\cdot\tilde{G}_{xx}(\alpha_n,\gamma,\beta)\cdot Z_1(\beta)\left(\frac{k}{k^2-\alpha_n^2}\right)^2\tau(\beta)\right\} \tag{1}$$

where

$$\tilde{G}_{xx}(\alpha_n,\gamma,\beta) = \frac{\alpha^2}{\alpha^2+\beta^2}Z^e + \frac{\beta^2}{\alpha^2+\beta^2}Z^h \tag{2}$$

is the longitudinal component of the dyadic Green's function in waveguide with specific boundary condition. Z^e and Z^h are eigenvalue equations of the LSE and LSM modes.
And

$$\begin{aligned} Z_1(\beta) &= \left[J_0(|\beta w|)\left(\frac{\cos\alpha_n x_1 - \cos kx_1}{\sin kx_1}\right)\right]^2 \\ \tau(\beta) &= \sin\beta z_1 \exp(-j\beta z_1) \\ \delta_n &= \begin{cases} 1 & \text{for } n=0 \\ 2 & \text{otherwise} \end{cases} \end{aligned}$$

In the above equation, β_{mn} are poles of $\tilde{G}_{xx}$, which satisfy the relation

$$\beta_{mn}^2 = k^2 + \gamma_{mn}^2 - \alpha_n^2, \quad \alpha_n = \frac{n\pi}{b}$$

Equation (1) gives the general input impedance of a microstrip probe that lies in the E-plane of a waveguide. This equation applies to all boundary conditions.

As for the PEC boundary conditions, assume the dielectric substrate is very thin, the Green's function simplifies to [16]

$$\tilde{G}_{xx}(\alpha_n,\gamma,\beta) = \frac{jR_0}{\gamma/k}\left[\frac{k^2-\alpha_n^2}{k^2}\right]\left(\frac{\sinh\gamma d\cdot\sinh\gamma(a-d)}{\sinh\gamma a}\right) \tag{3}$$

Substituting (3) in (1) and compute the limit, we can get the expression:

$$Z_p = \frac{-2jR_0}{abk}\sum_{n=0}^{+\infty}\delta_n\sum_{m=1}^{+\infty}\frac{(-1)^m}{\beta_{mn}}\cdot\sin\frac{m\pi d}{a}\sin\frac{m\pi(a-d)}{a}\frac{k^2}{k^2-\alpha_n^2}\cdot Z_1(\beta_{mn})\tau(\beta_{mn}) \tag{4}$$

The pole of $\tilde{G}_{xx}$ yields

$$\gamma_{mn} = \frac{jm\pi}{a}\gamma, \quad \beta_{mn} = \sqrt{k^2 - \left(\frac{m\pi}{a}\right)^2 - \left(\frac{n\pi}{b}\right)^2}$$

Now considering the PEC-PMC, we derived the Green's function in this boundary condition as follows:

Assume that the substrate is very thin. According to [15], the LSM (TM-to-x) and LSE (TE-to-x) equivalent transmission lines for the E-plane probe with PMC-PEC can be drawn in Figure 4. The PMC at $y = 0$ and PEC at $y = a$ are represented by open and short circuits at respective plane.

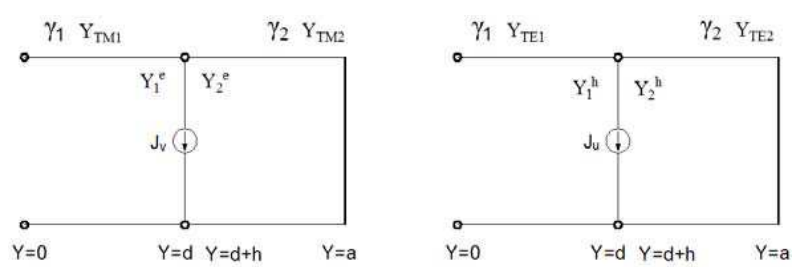

Figure 4. The LSM and LSE equivalent transmission lines model for the single probe in waveguide with PEC-PMC.

Here,

$$\gamma_i = \sqrt{\alpha_n^2 + \beta^2 - \varepsilon_i k^2} \tag{5a}$$

$$Y_{\mathrm{TM}i} = \frac{j\omega\varepsilon_i}{\gamma_i} \quad Y_{\mathrm{TE}i} = \frac{\gamma_i}{j\omega\mu_i} \quad i = 1, 2, \quad n = 0, 1, 2, \ldots \tag{5b}$$

The driving point input impedance Z^e and Z^h for the TM and TE equivalent circuit is given by:

$$Z^e = \frac{1}{Y_1^e + Y_2^e} \tag{6a}$$

$$Z^h = \frac{1}{Y_1^h + Y_2^h} \tag{6b}$$

where

$$Y_1^e = Y_{\mathrm{TM1}} \tanh \gamma_1 d \quad Y_2^e = Y_{\mathrm{TM2}} \coth \gamma_2 (a - d) \tag{7a}$$

$$Y_1^h = Y_{\mathrm{TE1}} \tanh \gamma_1 d \quad Y_2^h = Y_{\mathrm{TE2}} \coth \gamma_2 (a - d) \tag{7b}$$

In our design, the waveguide is filled with air, so

$$Y_{\mathrm{TM1}} = Y_{\mathrm{TM2}} = Y_{\mathrm{TM}} = \frac{j\omega\varepsilon_0}{\gamma} \quad Y_{\mathrm{TE1}} = Y_{\mathrm{TE2}} = Y_{\mathrm{TE}} = \frac{\gamma}{j\omega\mu_0} \tag{8}$$

$$Z^e = \frac{1}{Y_1^e + Y_2^e} = \frac{1}{Y_{\mathrm{TM}}} \cdot \frac{1}{\tanh \gamma d + \coth \gamma (a - d)} = \frac{1}{Y_{\mathrm{TM}}} \cdot \frac{\sinh \gamma (a - d) \cosh \gamma d}{\cosh \gamma a} \tag{9a}$$

$$Z^h = \frac{1}{Y_1^h + Y_2^h} = \frac{1}{Y_{\mathrm{TE}}} \cdot \frac{1}{\tanh \gamma d + \coth \gamma (a - d)} = \frac{1}{Y_{\mathrm{TE}}} \cdot \frac{\sinh \gamma (a - d) \sinh \gamma d}{\cosh \gamma a} \tag{9b}$$

Substituting (9a) and (9b) to (2) and after some algebraic manipulations, we can get the final expression:

$$\tilde{G}_{xx} (\alpha_n, \gamma, \beta) = \frac{jR_0}{\gamma/k} \left[\frac{k^2 - \alpha_n^2}{k^2} \right] \left(\frac{\cosh \gamma d \cdot \sinh \gamma (a - d)}{\cosh \gamma a} \right) \tag{10}$$

Substituting (10) in (1) and computing the limit, we can get the expression for PEC-PMC boundary conditions:

$$Z_p = \frac{-2jR_0}{abk} \sum_{n=0}^{+\infty} \delta_n \sum_{m=1}^{+\infty} \frac{(-1)^m}{\beta_{mn}} \cdot \cos \frac{(2m-1)}{2a} \pi d \cdot \sin \frac{(2m-1)}{2a} \pi (a - d) \cdot \frac{k^2}{k^2 - \alpha_n^2} \cdot Z_1 (\beta_{mn}) \tau (\beta_{mn}) \tag{11}$$

The pole of $\tilde{G}_{xx}$ yields

$$\gamma_{mn} = \frac{j(2m-1)\pi}{2a}, \quad \beta_{mn} = \sqrt{k^2 - \left(\frac{(2m-1)\pi}{2a} \right)^2 - \left(\frac{n\pi}{b} \right)^2}$$

To verifying our calculations, the input impedance of the single Wg-Ms probe was computed under two kinds of boundary conditions. The results were also validated by High Frequency Structure Simulator (HFSS). On both cases, the probes were fixed at middle plane of the waveguide broad-wall ($d = a/2$). Figure 5 shows the numerical data obtained from our equation and HFSS. In both case, data computed by the two methods show reasonable agreement from 26 to 40 GHz. The input resistances maintain fairly constant closely to Z_0 (characteristic impedance of the microstrip line) and the reactance remain slightly capacitive for the entire Ka-band. Data obtained by T. Q. Ho [17] are also presented under the PEC boundary condition in Figure 5(a) for comparison.

In order to match Z_p to Z_0, a high impedance line with length l is used in series with the probe to resonate out the capacitive reactance. The equivalent inductance of the high impedance line can be approximated as follows:

$$L \approx Z_h \cdot l \frac{\sqrt{\varepsilon_{eff}}}{c} (H) \tag{12}$$

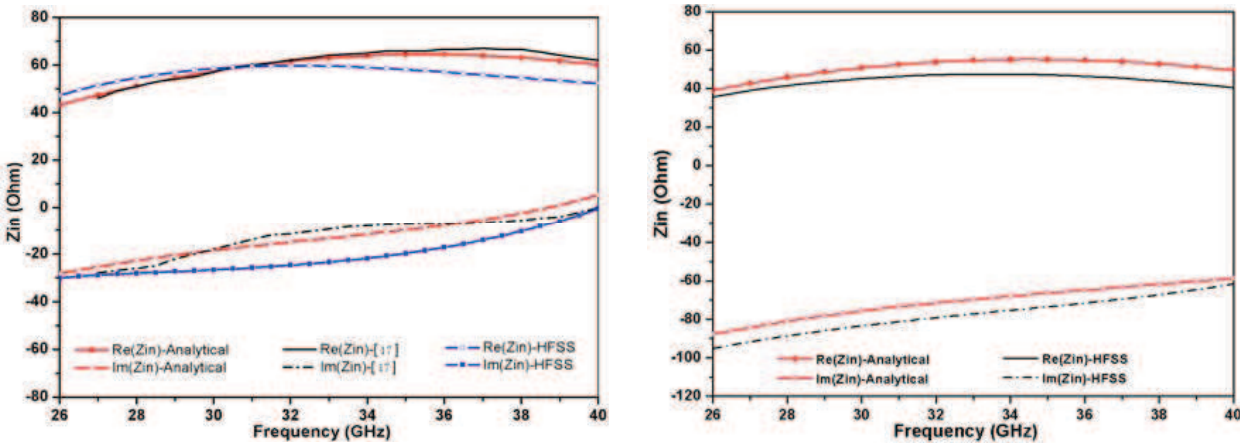

Figure 5. Input impedance of the single Wg-Ms probe versus frequency. (a) PEC boundary condition with $a = 7.12\,\text{mm}$, $b = 3.56\,\text{mm}$, $x_1 = 1.2\,\text{mm}$, $z_1 = 2.8\,\text{mm}$, $w = 0.187\,\text{mm}$. (b) PEC-PMC boundary condition with $a = 3.56\,\text{mm}$, $b = 1.78\,\text{mm}$, $x_1 = 1.2\,\text{mm}$, $z_1 = 2.6\,\text{mm}$, $w = 0.23\,\text{mm}$.

According to transmission-line theory [18], the input impedance Z_{in} can be calculated as follows:

$$Z_{in} = Z_p + jX_L \tag{13}$$

After the input impedance Z_{in} is obtained, the input reflection coefficient can be calculated as

$$\Gamma_{in} = \frac{Z_{in} - Z_0}{Z_{in} + Z_0} \tag{14}$$

2.2. Simulated Result

Once the initial dimensions of the microstrip probe, such as the length and width of the probe, are obtained using above equations, the whole two-way and four-way power divider/combiner can be optimized using HFSS for good input matching and low insertion loss. In our design, the microstrip probes and transmission lines were built on a 0.254 mm Rogers RT/Duroid 5880 substrate (relative permittivity of 2.2). Table 1 gives the values of some crucial parameters before and after the HFSS optimization. It can be seen that the dimensions computed by the analytical model are close to the optimum ones.

The optimized results of the 1×2 and 2×2 power divider/combiner are given in Figure 6 and Figure 7 respectively. In both case, the return losses of the waveguide ports are better than 20 dB from 24 to 40 GHz. For the 1×2 divider/combiner, the simulated insertion loss is better than 0.15 dB over the entire Ka-band, and the worst amplitude balance is 0.05 dB as shown in Figure 6(a). Figure 6(b) indicates that the phase difference between S_{21} and S_{31} is exactly 180°. For the 2×2 divider/combiner, the average insertion loss is less than 0.2 dB. Ports 2 and 3 (or ports 4 and 5) are in phase; port 2 (or port 3) and ports 4 (or port 5) are out of phase as analyzed before.

Table 1. Value of crucial parameter.

Parameter	X_1 (mm)	W (mm)	Z_1 (mm)	Z_h (Ω)	l (mm)
two-way before optimization	1.2	0.187	2.8	80	0.8
two-way after optimization	1.55	0.12	2.6	79	1.1
four-way before optimization	1.2	0.3	2.8	80	1.05
four-way after optimization	1.38	0.23	2.6	78	0.96

* l is calculated using Equation (12) at 33 GHz.

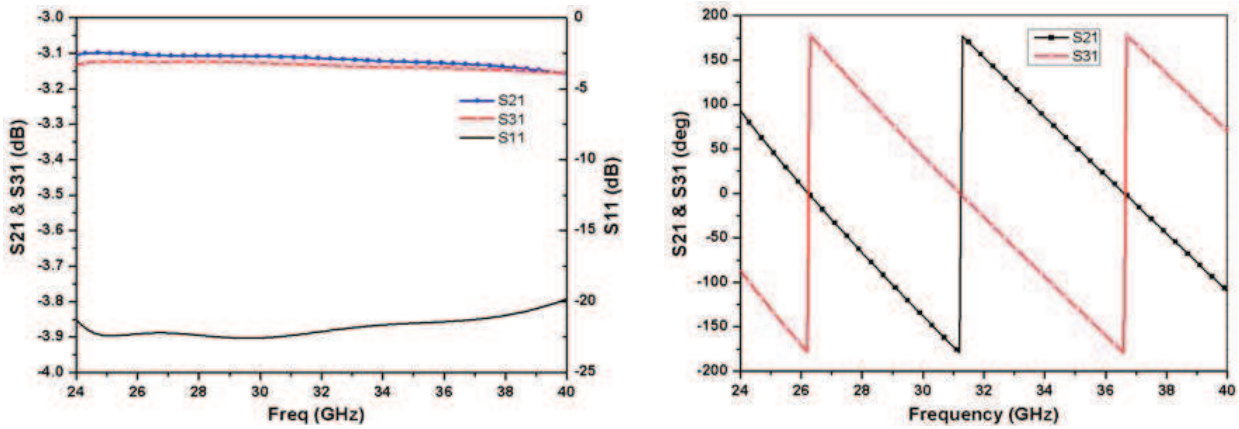

(a) (b)

Figure 6. The simulation results of the 1×2 power divider/combiner. (a) Return loss and insert loss. (b) Phases in degree.

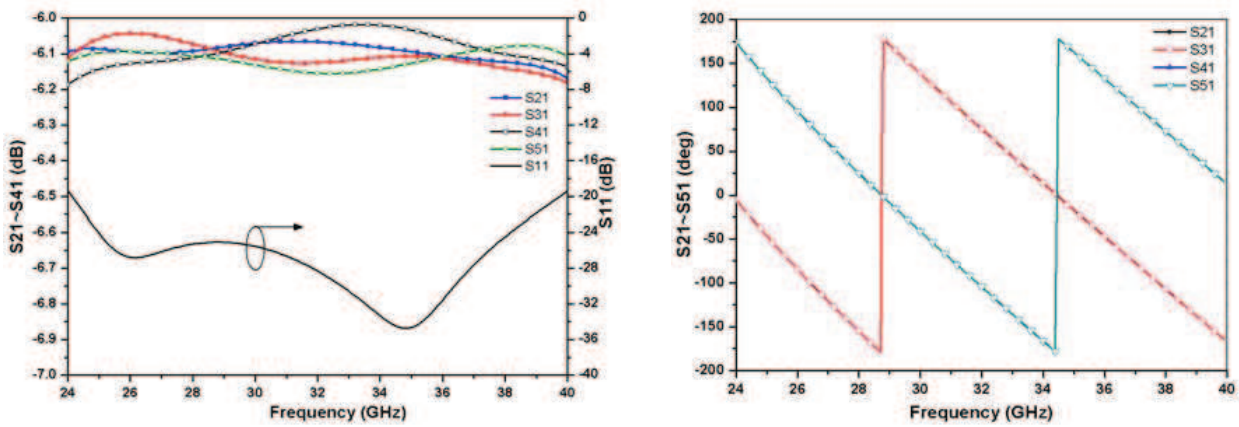

(a) (b)

Figure 7. The simulation results of the 2×2 power divider/combiner. (a) Return loss and insert loss. (b) Phases in degree.

3. EXPERIMENTAL PERFORMANCE

To experimentally evaluate the performance, 1×2 and 2×2 power divider/combiner were fabricated and measured. For convenient measurement, the divider and combiner are connected back-to-back with pieces of 40 mm long microstrip line. The waveguide housing was made of aluminum in E-plane split blocks type. The substrate ground plane was glued on the aluminum block channel using silver loaded epoxy. Dowel pins (1.6 mm diameter) were used to align the blocks. The two half blocks were screwed together to complete the fully assembled housing. EM absorber was used to eliminate potential cavity resonance and ensure stability. Photographs of the power divider-combiners are shown in Figure 8.

The measured insertion losses and return losses together with the simulated result of the 1×2 divider-combiner are shown in Figure 9(a). The measured insertion losses are less than 1.4 dB, including the losses in the 40 mm long microstrip lines. The return losses are better than 20 dB over the full Ka-band. Taking into account the theoretical microstrip losses (about 0.8 dB) and assuming a symmetrical back-to-back structure, the performance of a single 1×2 power divider/combiner can be approximated. Over the Ka-band, the insertion loss is less than 0.3 dB, which corresponds to a power combining

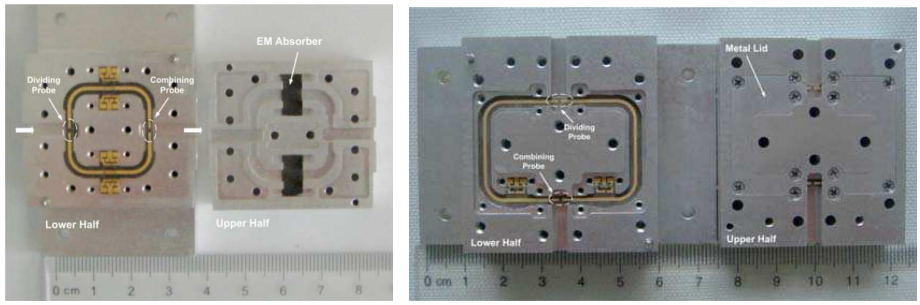

(a) (b)

Figure 8. Photographs of the (a) 1×2 back-to-back power divider-combiner and (b) 2×2 back-to-back power divider-combiner.

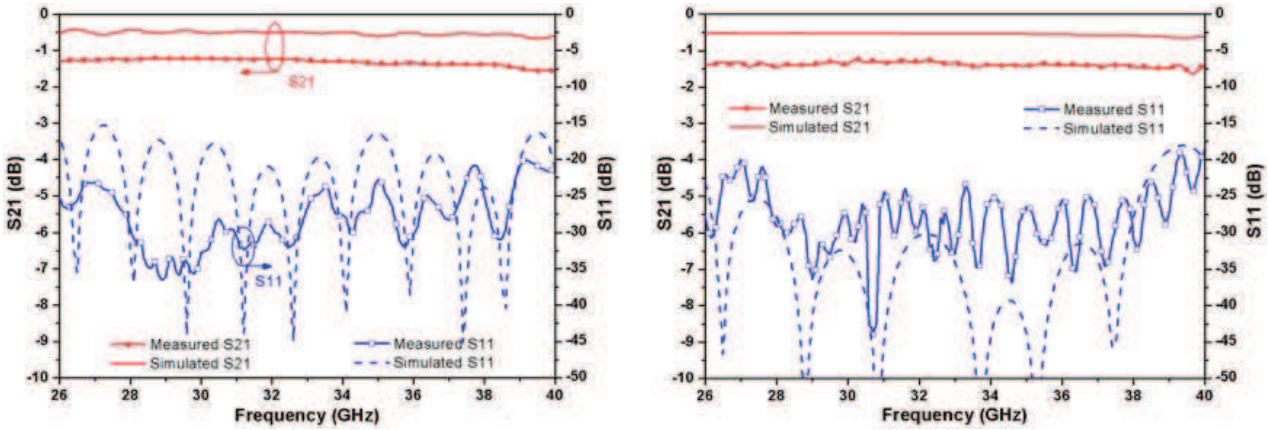

(a) (b)

Figure 9. Measured and simulated results of the back-to-back (a) 1×2 and (b) 2×2 power divider-combiner.

Table 2. Comparison of previously reported power combiner with this work.

Reference	Frequency Band (GHz)	Insertion Loss (dB)	Number of Device	Power Combining Type
[3]	32∼37	0.2	2	Binary circuit-level
[4]	31∼36	0.7	32	Waveguide-based Binary
[11]	26-32	0.6	2	Waveguide-Based Spatial
[13]	32∼38	0.4	4	Waveguide-Based Spatial
This work	26∼40	0.3	4	Waveguide-Based Spatial

efficiency higher than 93%. The measured frequency responses of the 2×2 divider-combiner are shown in Figure 9(b). The 2×2 divider exhibits an almost same performance as the 1×2 divider. No appreciable degradation in insertion loss and operating bandwidth is observed. Compared with the simulation results, the increased insertion loss is most likely attributed the surface roughness of the microstrip and the tolerance in manufacture and assembly. Nevertheless, the overall measured response show good agreement with the simulated results.

Table 2 demonstrates the comparison of the designed Ka-band power combiner with some of the reported Ka-band prototypes. The power combiner developed by our group is comparable to other power combiner in insertion loss while provides a much wider operating band.

4. CONCLUSION

A type of waveguide-based spatial power divider/combiner using improved Wg-Ms probe-array structure has been proposed in this paper. Based on the image theory and spectral domain method, general closed-form expressions for the input impedance of the Wg-Ms probe-array were established. Equivalent circuit model and efficient design method for this type of power divider/combiner were also developed. Ka-band two-way and four-way power divider/combiner have been designed, optimized, and measured. Both of the optimized power divider/combiner exhibits very low insertion loss, less than 0.3 dB over the entire Ka-band. A reasonable agreement between simulation and experiment was noted. In conclusion, this type of power combiner/divider demonstrates the advantages of full-band operation, low insertion loss and easy fabrication while maintaining compact size.

ACKNOWLEDGMENT

This work was supported by the National Natural Science Foundation of China (NSFC) under Grant No. 60921063. The authors wish to thank for the helpful discussions provided by Zhenghua Chen. The authors also would like to acknowledge Mrs. Sun for her assistance in circuit assembly.

REFERENCES

1. Chang, K. and C. Sun, "Millimeter-wave power-combining techniques," *IEEE Trans. Microwave Theory and Tech.*, Vol. 31, No. 2, 91–107, Feb. 1983.
2. Russell, K. J., "Microwave power combining techniques," *IEEE Trans. Microwave Theory and Tech.*, Vol. 27, No. 5, 472–478, May 1979.
3. Xie, X. Q., R. M. Xu, B. Yan, Y. Zhang, and W. G. Lin, "A novel millimeter-wave power combining circuit," *Int. J. Infrared and Millimeter Waves*, Vol. 26, No. 10, 1453–1464, 2005.
4. Epp, L. W., D. J. Hoppe, A. R. Khan, and S. L. Stride, "A high-power Ka-band (31–36 GHz) solid-state amplifier based on low-loss corporate waveguide combining," *IEEE Trans. Microwave Theory and Tech.*, Vol. 56, No. 8, 1899–1908, Aug. 2008.
5. Delisio, M. P. and R. A. York, "Quasi-optical and spatial power combining," *IEEE Trans. Microwave Theory and Tech.*, Vol. 50, No. 3, 929–936, Mar. 2002.
6. Kim, M., E. A. Sorvero, J. B. Hacker, M. P. DeLisio, J.-C. Chiao, S.-J. Li, D. Gagnon, J. J. Rosenberg, and D. B. Rutledge, "A 100-element HBT grid amplifier," *IEEE Trans. Microwave Theory and Tech.*, Vol. 41, No. 10, 1762–1770, Oct. 1993.
7. Chang, J., D. H. Schaubert, K. S. Yngvesson, J. Huang, V. Jamnejad, D. Rascoe, and A. L. Riley, "Ka-band power-combining MMIC array," *15th Int. Infrared Millimeter-Waves Conf. Dig.*, 532–534, Orlando, FL, Dec. 1990.
8. Tsai, H. S., M. J. W. Rodwell, and R. A. York, "Planar amplifier array with improved bandwidth using folded-slots," *IEEE Microwave and Guided Wave Letters*, Vol. 4, No. 4, 112–114, Apr. 1994.
9. Cheng, N. S., P. Jia, D. B. Rensh, and R. A. York, "A 120-W X-band spatially combined solid-state amplifier," *IEEE Trans. Microwave Theory and Tech.*, Vol. 47, No. 12, 2557–2561, Dec. 1999.
10. Chen, J. P., L.-Y. Chen, A. Alexanian, and R. A. York, "Broad-band high power amplifier using spatial power-combining technique," *IEEE Trans. Microwave Theory and Tech.*, Vol. 51, No. 12, 2469–2475, Dec. 2003.
11. Jeong, J., Y. Kwon, S. Lee, C. Cheon, and E. A. Sovero, "1.6- and 3.3-W power-amplifier modules at 24 GHz using waveguide-based power combining structures," *IEEE Trans. Microwave Theory and Tech.*, Vol. 48, No. 12, 2700–2708, Dec. 2000.
12. Song, K., Y. Fan, and X. Zhou, "Broadband radial waveguide power amplifier using a spatial power combining technique," *IET Microwaves, Antennas and Propagation*, Vol. 3, No. 8, 1179–1185, 2009.
13. Xie, X. Q., C. Zhao, and R. Diao, "A millimeter-wave power combining amplifier based on a waveguide-microstrip E-plane dual-probe four-way power combining network," *Int. J. Infrared and Millimeter Waves*, Vol. 29, No. 9, 862–870, 2008.

14. Shih, Y. C., T. N. Ton, and L. Q. Bui, "Waveguide-to-microstrip transitions for millimeter-wave applications," *IEEE MTT-S Int. Microwave Symp. Dig.*, Vol. 1, 473–475, May 1988.
15. Itoh, T., "Spectral domain immittance approach for dispersion characteristics of generalized printed transmission lines," *IEEE Trans. on Microwave Theory and Tech.*, Vol. 28, No. 7, 733–736, Jul. 1980.
16. Yassin, G. and S. Withington, "Analytical expression for the input impedance of a microstrip probe in waveguide," *Int. J. Infrared and Millimeter Waves*, Vol. 17, No. 10, 1685–1705, 1996.
17. Ho, T. Q. and Y.-C. Shih, "Spectral-domain analysis of E-plane waveguide to microstrip transition," *IEEE Trans. Microwave Theory and Tech.*, Vol. 37, No. 2, 388–392, Feb. 1989.
18. Pozar, D. M., *Microwave Engineering,* 2nd Edition, Wiley, New York, 1998.